Accessing the real part of the forward $J/\psi - p$ scattering amplitude from J/ψ photoproduction on protons around threshold

Oleksii Gryniuk and Marc Vanderhaeghen

Institut für Kernphysik & PRISMA Cluster of Excellence, Johannes Gutenberg Universität, D-55099 Mainz, Germany

We provide an updated analysis of the forward J/ψ-p scattering amplitude, relating its imaginary part to $\gamma p \to J/\psi p$ and $\gamma p \to c\bar{c} X$ cross section data, and calculating its real part through a once-subtracted dispersion relation. From a global fit to both differential and total cross section data, we extract a value for the spin-averaged J/ψ-p s-wave scattering length $a_{\psi p} = 0.046 \pm 0.005$ fm, which can be translated into a J/ψ binding energy in nuclear matter of $B_\psi = 2.7 \pm 0.3$ MeV. We estimate the forward-backward asymmetry to the $\gamma p \to e^- e^+ p$ process around the J/ψ resonance, which results from interchanging the leptons in the interference between the J/ψ production and the Bethe-Heitler mechanisms. We show that to good approximation this asymmetry depends linearly on $a_{\psi p}$, and can reach values around -25% for forthcoming J/ψ threshold production experiments at Jefferson Lab. Its measurement can thus provide a very sensitive observable for a refined extraction of $a_{\psi p}$.

I. INTRODUCTION

The interaction between heavy quarkonia, such as J/ψ, and protons or nuclear matter has generated a lot of interest over the past decades as it provides a unique setting to test the gluonic van der Waals interaction in quantum chromodynamics (QCD). As valence light-quark exchange between the J/ψ and the nuclear system cannot occur, and light-quark antiquark exchange is strongly suppressed due to the Okubo-Zweig-Iizuka rule, the interaction proceeds dominantly through multiple gluon exchange which provides a weakly attractive interaction. As the heavy quarkonium is a small size system, it can be treated as a color dipole, and its interaction with the nucleon or nucleus may be estimated from the knowledge of its chromoelectric polarizability; see Refs. [1–3] for reviews and references therein. For nuclei, this attraction may be strong enough to provide a bound state between the $c\bar{c}$ state and the nucleus [4–6]. Using a perturbative calculation for the chromoelectric polarizability of a heavy quarkonium [7] and a two-gluon exchange interaction, Ref. [6] estimated a binding energy for a J/ψ in nuclear matter $B_\psi \sim 10$ MeV. In subsequent works, also higher-order nonperturbative modifications to the interaction between quarkonia and nucleons and nuclei were explored, including the coupling of the J/ψ to $D\bar{D}$, $D\bar{D}^*$ and $D^*\bar{D}^*$ intermediate states [8–10], which may also lead to attractive interactions. The latter work [10] predicted J/ψ binding energies ranging from around 5 MeV in ^{4}He to around 15–20 MeV in ^{208}Pb.

The quantitative study of a possible formation of such bound states requires a more precise knowledge of the J/ψ-nucleon interaction at low energies, which may be characterized by its (spin-independent) s-wave scattering length $a_{\psi p}$, corresponding to a J/ψ-proton (p) total cross section

at the threshold of $\sigma_{\psi p} \equiv 4\pi a_{\psi p}^2$. In the absence of a J/ψ-p bound state, a small positive (negative) value of $a_{\psi p}$ would indicate a weakly attractive (repulsive) J/ψ-p interaction. If the attraction is sufficiently strong, it may then support J/ψ-nuclear bound states [11]. It has been estimated using QCD sum rules [12] that $a_{\psi p} \sim 0.1$ fm, corresponding with $\sigma_{\psi p} \sim 1.26$ mb. Calculations based on the rather uncertain value of the J/ψ chromoelectric polarizability [13] provide estimates for $a_{\psi p}$ ranging between a value of $a_{\psi p} = 0.05$ fm [14] at the lower end, and a value of $a_{\psi p} = 0.37$ fm [15] at the higher end. The latter value would lead to J/ψ binding energy in nuclear matter exceeding 20 MeV.

In recent years, the question whether J/ψ-nuclear bound states exist became also amenable to lattice QCD calculations [16–18]. The most recent of these studies [18] inferred a charmonium-nuclear matter binding energy $B_\psi \lesssim 40$ MeV. The current lattice calculations were however performed at large pion masses ($m_\pi \sim 805$ MeV), and it is possible that the systems involving the lightest nuclei will therefore be unbound at the physical pion mass. Future calculations for smaller quark masses are clearly called for.

The J/ψ-p interaction was furthermore studied in Refs. [19,20] as a probe of the color deconfinement in high-energy nucleus-nucleus collisions. Based on the small size of the J/ψ, around $r_\psi \sim 0.2$ fm $\ll \Lambda_{\text{QCD}}^{-1}$, the J/ψ-p cross section was estimated in those works in terms of the gluon distribution in the nucleon and related through vector meson dominance (VMD) to the J/ψ photoproduction cross section on the proton. Using different parametrizations of the gluon distributions in a proton from deep inelastic scattering, the experimental behavior of the cross section was well reproduced in Ref. [20]. In a related

work [21], by using VMD and using data for hidden and open charm photoproduction on a proton as input, a phenomenological estimate of the J/ψ-p elastic cross section was given. In the present work, we provide an update along these lines, with the aim to provide an improved extraction of the threshold J/ψ-p scattering amplitude. For this purpose we evaluate the J/ψ-p forward scattering amplitude in a dispersive formalism. As in Ref. [21], we constrain the imaginary part from the present world data of hidden and open-charm photoproduction. The real part is evaluated through a dispersion relation, which involves one subtraction constant, which can be related to $a_{\psi p}$. We are able to substantially improve the precision of the fit, by including the forward differential cross section data for $\gamma p \to J/\psi p$ in the fit, and study the sensitivity of the $\gamma p \to J/\psi p$ cross section in the threshold region to the subtraction constant. This then allows us to make a quantitative study for planned experiments at the Jefferson Laboratory (JLab) [22–24], which are aimed to measure the $\gamma p \to J/\psi p$ process in the threshold region.

The paper is organized as follows. We describe the forward J/ψ-p scattering amplitude in Sec. II, relating its imaginary part to $\gamma p \to J/\psi p$ and $\gamma p \to c\bar{c}X$ data. We subsequently calculate the real part from a dispersion relation, involving one subtraction constant. In our framework, the six parameters describing the discontinuities and the one subtraction constant are obtained from a global fit to both total and forward differential photoproduction cross sections. In Sec. III, we then start from this $\gamma p \to J/\psi p$ amplitude to describe the $\gamma p \to J/\psi p \to e^- e^+ p$ process, and calculate the forward-backward asymmetry for the $\gamma p \to e^- e^+ p$ process around the J/ψ resonance, which results from interchanging the leptons in the interference between the J/ψ production mechanism and the competing Bethe-Heitler (BH) mechanism. We show that this forward-backward asymmetry, which is proportional to the real part of the J/ψ-p amplitude, provides a very sensitive observable to extract the subtraction constant in the forward J/ψ-p scattering amplitude, which in turn allows us to extract $a_{\psi p}$. We present results for this forward-backward asymmetry, including error bands resulting from our fitting procedure, in the kinematics of planned experiments at JLab. Finally we provide our conclusions in Sec. IV.

II. FORWARD $J/\psi - p$ SCATTERING AMPLITUDE and $\gamma p \to J/\psi p$ PROCESS

We consider the forward J/ψ-p elastic scattering process, which is described by the spin-averaged forward scattering amplitude $T_{\psi p}(\nu)$, where the shorthand ψ denotes the J/ψ state. The amplitude $T_{\psi p}$ depends on the crossing variable ν, defined in terms of the Mandelstam invariants as

$$\nu \equiv \frac{s-u}{4} = \frac{1}{2}(s - M^2 - M_\psi^2), \qquad (1)$$

where $M(M_\psi)$ stand for the masses of the proton (ψ), respectively.

The forward differential cross section for the $\psi p \to \psi p$ process can then be expressed as

$$\left.\frac{d\sigma}{dt}\right|_{t=0}(\psi p \to \psi p) = \frac{1}{64\pi s q_{\psi p}^2}|T_{\psi p}(\nu)|^2, \qquad (2)$$

where in the forward direction the momentum transfer $t = 0$, and where $q_{\psi p}$ denotes the magnitude of the ψ three-momentum in the c.m. frame, given by

$$q_{\psi p}^2 = \frac{1}{4s}[s - (M_\psi + M)^2][s - (M_\psi - M)^2]. \qquad (3)$$

The optical theorem relates the imaginary part of $T_{\psi p}(\nu)$ to the $\psi p \to X$ total cross section $\sigma_{\psi p}^{\text{tot}}$ as

$$\Im T_{\psi p}(\nu) = 2\sqrt{s} q_{\psi p} \sigma_{\psi p}^{\text{tot}}(\nu). \qquad (4)$$

The amplitude $T_{\psi p}(\nu)$ has the property that it is even under crossing, i.e. $T_{\psi p}(-\nu) = T_{\psi p}(\nu)$. The real part of the amplitude $T_{\psi p}(\nu)$ can be reconstructed from the knowledge of the imaginary part along the real ν axis using a dispersion relation, provided the integral converges. For large ν, the amplitude is diffractive following approximately the behavior $\Im T_{\psi p}(\nu) \sim \nu^a$, with $1 \leq a < 2$. The convergence of the dispersion integral therefore requires one subtraction. This leads to the subtracted dispersion relation,

$$\Re T_{\psi p}(\nu) = T_{\psi p}(0) + \frac{2}{\pi}\nu^2 \int_{\nu_{\text{el}}}^\infty d\nu' \frac{1}{\nu'} \frac{\Im T_{\psi p}(\nu')}{\nu'^2 - \nu^2}, \quad (5)$$

where $\nu_{\text{el}} \equiv M M_\psi$ corresponds with the elastic threshold $s = s_{\text{el}} = (M_\psi + M)^2 = 16.28 \,\text{GeV}^2$. Furthermore in Eq. (5), the real subtraction constant $T_{\psi p}(0)$ denotes the amplitude at $\nu = 0$. This subtraction constant can be predicted in models, see e.g. [20], or has to be obtained from lattice QCD. Alternatively, we can use it as a fit parameter and extract it from data. In the following, we show the sensitivity to extract this subtraction constant from the measurement of the $\gamma p \to \psi p$ process in the threshold region, and relate it with the ψ-p s-wave scattering length $a_{\psi p}$.

Physically, the discontinuity of the amplitude $T_{\psi p}(\nu)$ entering the integrand of Eq. (5) has two contributions: an elastic cut starting at s_{el}, and an inelastic contribution corresponding with open-charm (meson) production on the proton. We parametrize the inelastic contribution to $T_{\psi p}$ by an effective inelastic cut which starts at the $D\bar{D}$ meson production threshold, corresponding with

$s_{\text{inel}} = (M + 2M_D)^2 = 21.79 \text{ GeV}^2$, or equivalently $\nu_{\text{inel}} = 5.66 \text{ GeV}^2$. The imaginary part of $T_{\psi p}$ is then obtained as a sum of elastic and inelastic discontinuities,

$$\Im T_{\psi p}(\nu) = \theta(\nu - \nu_{\text{el}}) \text{Disc}_{\text{el}} T_{\psi p}(\nu)$$
$$+ \theta(\nu - \nu_{\text{inel}}) \text{Disc}_{\text{inel}} T_{\psi p}(\nu). \quad (6)$$

We parametrize the elastic and inelastic discontinuities by the following three-parameter forms:

$$\text{Disc}_{\text{el}} T_{\psi p}(\nu) = C_{\text{el}} \left(1 - \frac{\nu_{\text{el}}}{\nu}\right)^{b_{\text{el}}} \left(\frac{\nu}{\nu_{\text{el}}}\right)^{a_{\text{el}}} \quad (7)$$

$$\text{Disc}_{\text{inel}} T_{\psi p}(\nu) = C_{\text{inel}} \left(1 - \frac{\nu_{\text{inel}}}{\nu}\right)^{b_{\text{inel}}} \left(\frac{\nu}{\nu_{\text{inel}}}\right)^{a_{\text{inel}}}, \quad (8)$$

where the factors $\sim (1 - \nu_{\text{thr}}/\nu)^b$ determine the behavior around the respective threshold ν_{thr}, and the factors $\sim \nu^a$ determine the Regge behavior of the amplitude at large ν. In the following we discuss how we can determine the respective parameters appearing in the elastic and inelastic discontinuities.

The discontinuity across the elastic cut, Disc_{el}, is related through the optical theorem to the $\psi p \rightarrow \psi p$ elastic scattering cross section $\sigma_{\psi p}^{\text{el}}$ as

$$\text{Disc}_{\text{el}} T_{\psi p}(\nu) = 2\sqrt{s} q_{\psi p} \sigma_{\psi p}^{\text{el}}. \quad (9)$$

We use the VMD assumption to relate the elastic cross section $\sigma_{\psi p}^{\text{el}}$ to the $\gamma p \rightarrow \psi p$ cross section [21,25],

$$\sigma_{\psi p}^{\text{el}} = \left(\frac{M_\psi}{e f_\psi}\right)^2 \left(\frac{q_{\gamma p}}{q_{\psi p}}\right)^2 \sigma(\gamma p \rightarrow \psi p), \quad (10)$$

with electric charge e given through $\alpha = e^2/(4\pi) \simeq 1/137$, and where f_ψ is the ψ decay constant, which is obtained from the $\psi \rightarrow e^+ e^-$ decay as

$$\Gamma_{\psi \rightarrow ee} = \frac{4\pi\alpha^2}{3} \frac{f_\psi^2}{M_\psi}. \quad (11)$$

The experimental value $\Gamma_{\psi \rightarrow ee} = 5.55 \text{ keV}$ yields $f_\psi = 0.278 \text{ GeV}$. Furthermore, $q_{\gamma p}$ denotes the magnitude of the γ three-momentum in the c.m. frame of the $\gamma p \rightarrow \psi p$ process,

$$q_{\gamma p} = \frac{(s - M^2)}{2\sqrt{s}}. \quad (12)$$

Equations (7), (9) and (10) then yield the parametrization for the $\gamma p \rightarrow \psi p$ total cross section,

$$\sigma(\gamma p \rightarrow \psi p) = \left(\frac{e f_\psi}{M_\psi}\right)^2 \frac{C_{\text{el}}}{2\sqrt{s} q_{\gamma p}} \left(\frac{q_{\psi p}}{q_{\gamma p}}\right)$$
$$\times \left(1 - \frac{\nu_{\text{el}}}{\nu}\right)^{b_{\text{el}}} \left(\frac{\nu}{\nu_{\text{el}}}\right)^{a_{\text{el}}}. \quad (13)$$

The discontinuity across the inelastic cut, $\text{Disc}_{\text{inel}}$, is related through the optical theorem to the $\psi p \rightarrow c\bar{c}X$ inelastic cross section $\sigma_{\psi p}^{\text{inel}}$ as

$$\text{Disc}_{\text{inel}} T_{\psi p}(s) = 2\sqrt{s} q_{\psi p} \sigma_{\psi p}^{\text{inel}}. \quad (14)$$

Using again VMD allows us to relate the inelastic cross section $\sigma_{\psi p}^{\text{inel}}$ to the $\gamma p \rightarrow c\bar{c}X$ cross section, with an analogous relation as in Eq. (10),

$$\sigma_{\psi p}^{\text{inel}} = \left(\frac{M_\psi}{e f_\psi}\right)^2 \left(\frac{q_{\gamma p}}{q_{\psi p}}\right)^2 \sigma(\gamma p \rightarrow c\bar{c}X). \quad (15)$$

Equations (8), (14) and (15) then yield the parametrization for the $\gamma p \rightarrow c\bar{c}X$ total cross section,

$$\sigma(\gamma p \rightarrow c\bar{c}X) = \left(\frac{e f_\psi}{M_\psi}\right)^2 \frac{C_{\text{inel}}}{2\sqrt{s} q_{\gamma p}} \left(\frac{q_{\psi p}}{q_{\gamma p}}\right)$$
$$\times \left(1 - \frac{\nu_{\text{inel}}}{\nu}\right)^{b_{\text{inel}}} \left(\frac{\nu}{\nu_{\text{inel}}}\right)^{a_{\text{inel}}}. \quad (16)$$

Having fixed the imaginary part of the ψ-p forward scattering amplitude, we then calculate its real part using the subtracted dispersion relation of Eq. (5). With the knowledge of the real and imaginary parts of the forward scattering amplitude $T_{\psi p}$, we can determine the forward ($t = 0$) differential cross section for the $\gamma p \rightarrow \psi p$ process using VMD,

$$\frac{d\sigma}{dt}\bigg|_{t=0} (\gamma p \rightarrow \psi p) = \left(\frac{e f_\psi}{M_\psi}\right)^2 \left(\frac{q_{\psi p}}{q_{\gamma p}}\right)^2 \frac{d\sigma}{dt}\bigg|_{t=0} (\psi p \rightarrow \psi p)$$
$$= \left(\frac{e f_\psi}{M_\psi}\right)^2 \frac{1}{64\pi s q_{\gamma p}^2} |T_{\psi p}(\nu)|^2. \quad (17)$$

Note that on the lhs of Eq. (17) the $\gamma p \rightarrow \psi p$ differential cross section is obtained at the unphysical point $t = 0$. Its experimental determination thus requires an extrapolation from $t = t_{\text{min}}$ to $t = 0$.

Our formalism has seven parameters: three parameters describing the elastic discontinuity, three describing the inelastic discontinuity, and the subtraction constant $T_{\psi p}(0)$. We obtain the values for these seven parameters [$T_{\psi p}(0)$, $a_{\text{el/inel}}$, $b_{\text{el/inel}}$, $c_{\text{el/inel}}$] by simultaneously fitting the available data for $\sigma(\gamma p \rightarrow \psi p)$, $\sigma(\gamma p \rightarrow c\bar{c}X)$ and $d\sigma/dt|_{t=0}(\gamma p \rightarrow \psi p)$. For this purpose we use the Levenberg-Marquardt algorithm [26,27] of the nonlinear least-squares optimization procedure implemented in MINPACK [28]. For our fits we estimate the error based

on a covariance matrix for the parameters and a linear uncertainty propagation for each of the functions. The covariance matrix Σ_p is obtained based on the experimental uncertainties of the data values as follows:

$$\Sigma_p = (\mathbf{J}_f^{\mathrm{T}} \cdot \Sigma_e^{-1} \cdot \mathbf{J}_f)^{-1}, \qquad \mathrm{J}_f^{(i,j)} = \frac{\partial f}{\partial p_j}(W_i),$$

$$\Sigma_e^{(i,j)} = \delta^{(i,j)}(\sigma_e^i)^2, \tag{18}$$

where W_i is the W-value of the ith data point (with $s = \mathrm{W}^2$), σ_e^i is the total experimental uncertainty of the ith data point, and f is the fit function of interest which depends on the energy variable (W) and the set of seven parameters ($\{p\}$). The derivatives over the parameters are taken at their fitted values.

We show our fit to the $\gamma p \to \psi p$ ($\gamma p \to c\bar{c}X$) total cross section world data in Fig. 1 (Fig. 2) respectively as a function of the c.m. energy W. By comparing Figs. 1 and 2 one notices that the ratio of the inelastic over elastic cross sections $\sigma(\gamma p \to c\bar{c}X)/\sigma(\gamma p \to \psi p)$ is around a factor of 30–50. Therefore, the inelastic discontinuity dominates the determination of the forward ψ-p amplitude. Furthermore, we show the forward differential cross section for the $\gamma p \to \psi p$ process in Fig. 3 for three values of the subtraction constant $T_{\psi p}(0)$. We note that the few HERA data points for the inelastic cross section in Fig. 2 at the highest energies ($W > 100$ GeV) are not so well reproduced. However, these data points only marginally influence the fit, which in this region is mainly driven by the precise forward differential cross section data of Fig. 3. Our global fit yields the parameters for the elastic and inelastic discontinuities shown in Table I (second column, $x = $ el;

FIG. 2. W-dependence of the $\gamma p \to c\bar{c}X$ total cross section. The data are from SLAC [35], Fermilab [36], EMC [37], CERN/WA58 [38], and HERA/ZEUS [39]. The curve and band is the result of our global fit using Eq. (16) with parameters given in Table I (third column, $x = $ inel).

third column, $x = $ inel). For the subtraction constant we obtain the fitted value of $T_{\psi p}(0) = 22.45 \pm 2.45$. As an indicator of the quality of our fit, we evaluated the reduced chi-squared,

$$\chi_{\mathrm{red}}^2 = \chi^2/(N_{\mathrm{d}} - N_{\mathrm{p}}), \tag{19}$$

FIG. 3. W-dependence of the $\gamma p \to J/\psi p$ differential cross section, extrapolated to the forward direction ($t = 0$), for different values of the subtraction constant $T_{\psi p}(0)$ in the forward ψ-p scattering amplitude. The data are from SLAC [30], CERN/EMC [40], Fermilab [31], and HERA [34]. The black curve $T_{\psi p}(0) = 22.45$ shows the best fit value, with a corresponding error band resulting from our fitting procedure.
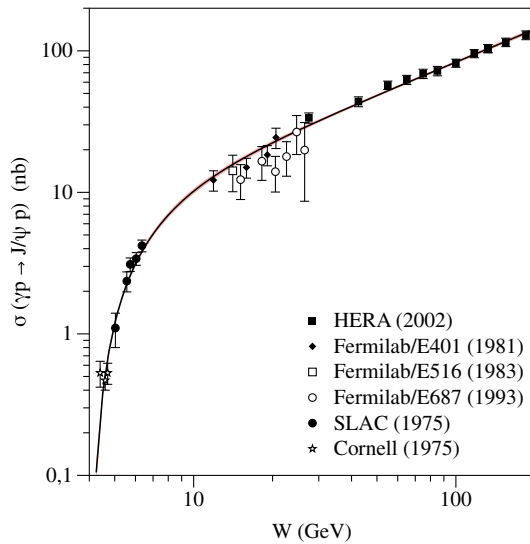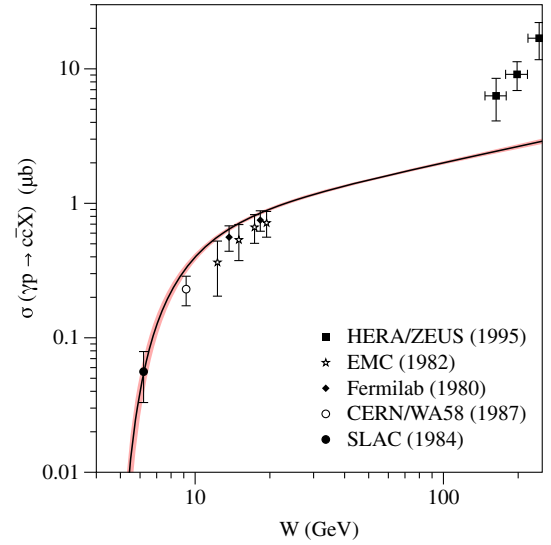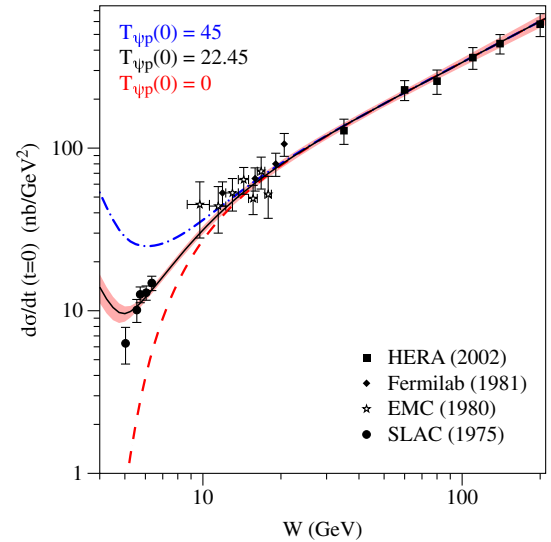

FIG. 1. W-dependence of the $\gamma p \to J/\psi p$ total cross section. The data are from Cornell [29], SLAC [30], Fermilab [31–33], and HERA [34]. The curve and band is the result of our global fit using Eq. (13) with parameters given in Table I (second column, $x = $ el).

TABLE I. Fit results for the coefficients entering the elastic discontinuity (second column, $x = $ el) of Eq. (7), and the inelastic discontinuity (third column, $x = $ inel) of Eq. (8).

	$x = $ el	$x = $ inel
C_x	0.10 ± 0.01	20.51 ± 1.70
b_x	1.27 ± 0.17	3.53 ± 0.66
a_x	1.38 ± 0.01	1.20 ± 0.01

with N_d being the total number of the data points we use in our fitting procedure and N_p being the number of fitting parameters. With the values of $N_d = 62$ and $N_p = 7$, we get $\chi^2_{red} = 1.36$. Its value shows that the present fit is decent (i.e. one is not overfitting) although not perfect, indicating the lack of a sufficient rich database. Forthcoming more precise data especially in the threshold region, as expected from the planned JLab experiments [22–24], will have a strong impact on the quality of such a fit.

We also note that the $\gamma p \to \psi p$ reaction in the threshold region might by modified due to the presence of pentaquark resonances, which have recently been reported by the LHCb Collaboration [41]. A new experiment at JLab [24] aims to search for such resonances in the $\gamma p \to \psi p$ reaction in the threshold region. If a sizable excitation strength of such pentaquark states in the $\gamma p \to \psi p$ threshold cross section is present, it was estimated in Ref. [24], based on a model calculation [42], that this would most likely occur at larger values of $-t$, away from the forward region, and thus not influence our analysis. If, on the other hand, such resonances yield sizeable excitation strength in the forward region, they could be added to the parametrization of the elastic discontinuity. The dispersion relation of Eq. (5) would then allow us to quantify the change to the real part of the forward ψ-p amplitude.

We show the real and imaginary parts of $T_{\psi p}$ in Fig. 4 for our best fit value of the subtraction constant $T_{\psi p}(0) = 22.45$, as well as for two values around this: $T_{\psi p}(0) = 0$ and $T_{\psi p}(0) = 45$. We notice that for $W < 10$ GeV the real part dominates over the imaginary part, whereas at very high energies ($W \gg 10$ GeV) the amplitude is largely dominated by the imaginary part, as expected for a diffractive process.

We can relate the forward ψ-p amplitude at threshold, $T_{\psi p}(\nu = \nu_{el})$, corresponding with $\sqrt{s} = M + M_\psi$, with the value of the ψ-p s-wave scattering length, $a_{\psi p}$, defined as

$$T_{\psi p}(\nu = \nu_{el}) = 8\pi(M + M_\psi)a_{\psi p}, \quad (20)$$

where our sign definition of $T_{\psi p}$ is fixed by Eq. (4). Note that in this convention, in the absence of a ψ-p bound state, a positive (negative) value of $a_{\psi p}$ corresponds to a positive (negative) s-wave phase shift, describing low-energy scattering from a weakly attractive (repulsive) potential.
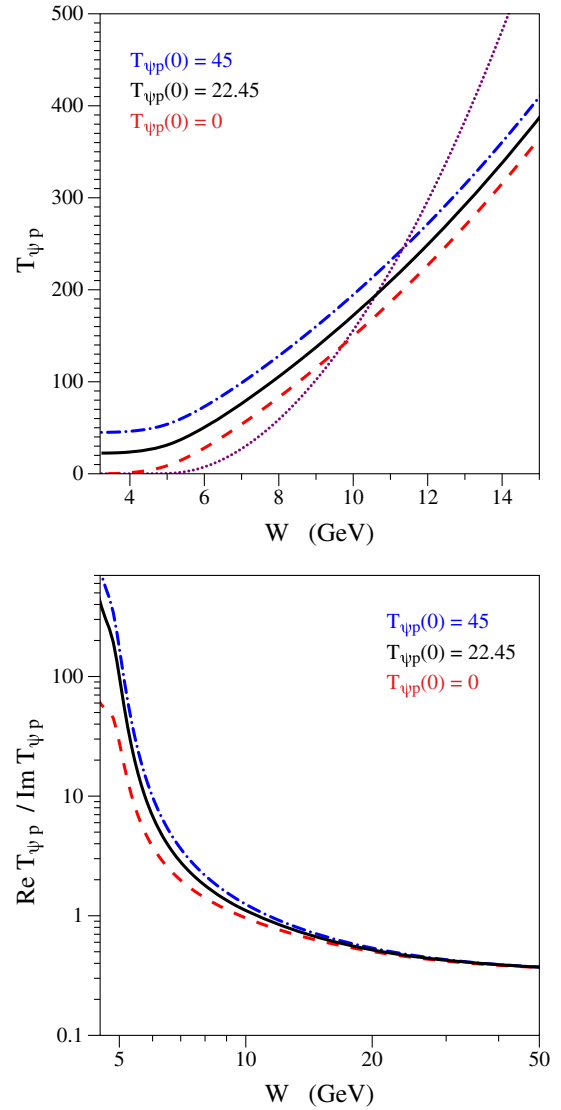

FIG. 4. Upper panel: Imaginary part (dotted curve) and real part of the forward scattering amplitude $T_{\psi p}$ as a function of W. The real part is shown for three values of the subtraction constant as indicated on the figure. Lower panel: Corresponding ratios of real over imaginary parts.

Using the dispersion relation Eq. (5) to relate $T_{\psi p}(0)$ with $T_{\psi p}(\nu_{el})$, we show the corresponding scattering lengths for three choices of the subtraction constant in Table II. Note that our best fit value $T_{\psi p}(0) = 22.45$ results in a ψ-p scattering length $a_{\psi p} \sim 0.05$ fm, which is at the lower end of the range of values estimated in the literature, ranging from $a_\psi = 0.05$ fm [14] to $a_\psi = 0.37$ fm [15]. The value $a_{\psi p} \sim 0.05$ fm corresponds with a threshold ψ-p total cross section of $\sigma_{\psi p} \sim 0.3$ mb.

In a linear density approximation, the ψ-p scattering length $a_{\psi p}$ can be related to the ψ binding energy in nuclear matter, B_ψ, corresponding with the depth of the potential well seen by ψ in nuclear matter, as [14]

TABLE II. Values of the subtraction term $T_{\psi p}(0)$ (first column), the corresponding values of the threshold amplitude $T_{\psi p}(\nu_{\text{el}})$ (second column), the corresponding ψ-p s-wave scattering lengths $a_{\psi p}$ (third column), and the corresponding ψ-nuclear matter binding energy B_ψ, according to Eq. (21) (fourth column).

| $T_{\psi p}(0)$	$T_{\psi p}(\nu = \nu_{\text{el}})$	$a_{\psi p}$ (in fm)	B_ψ (in MeV)
0	1.30	0.003	0.2
22.45 ± 2.45	23.74 ± 2.59	0.046 ± 0.005	2.7 ± 0.3
45	46.30	0.090	5.2

$$B_\psi \simeq \frac{8\pi(M + M_\psi)a_{\psi p}}{4MM_\psi}\rho_{nm}, \qquad (21)$$

where $\rho_{nm} \simeq 0.17$ fm^{-3} denotes the nuclear matter density. We show the B_ψ values corresponding with the three values of $T_{\psi p}(0)$ considered in our calculations in Table II (last column). Our best fit value $a_{\psi p} \sim 0.05$ fm thus corresponds to a ψ binding energy in nuclear matter of $B_\psi \sim 3$ MeV.

III. FORWARD-BACKWARD ASYMMETRY IN THE $\gamma p \to \psi p \to e^- e^+ p$ PROCESS

The value of $T_{\psi p}(0)$ extracted in the previous section is mainly sensitive to the forward differential cross section of the $\gamma p \to \psi p$ process in the threshold region. The experimental access of the $\gamma p \to \psi p$ process proceeds through the reconstruction of the decay $\psi \to e^- e^+$ (or $\psi \to \mu^- \mu^+$), shown in Fig. 5 (left). In the threshold region in the forward direction (at a small value of $-t$), one may have a significant interference with the competing Bethe-Heitler mechanism, shown in Fig. 5 (right), which results in the same final state. We study this interference in this section, and exploit it to find an observable which depends linearly on $T_{\psi p}(0)$.

For this purpose, we calculate the observables for the process $\gamma(q, \lambda) + p(p, s_p) \to e^-(l_-, s_-) + e^+(l_+, s_+) + p(p', s'_p)$ (Fig. 5, left), with q, p, p', l_-, l_+ being the four-momenta of initial photon, initial proton, final proton, final electron and positron, respectively, and where λ, s_p, s'_p, s_-, s_+ are the corresponding helicities. In the following expressions we denote the average nucleon four-momentum by $P = (p' + p)/2$, the four-momentum of the $e^- e^+$ pair as $q' = l_- + l_+$, the invariant mass squared of the dilepton pair as $M_{ll}^2 = q'^2$, and indicate the squared
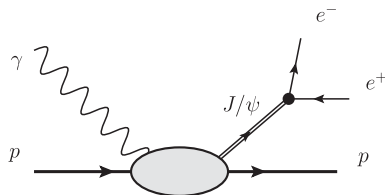
momentum transfer between initial and final protons as $t = (p' - p)^2$.

For small values of $-t$, the near-forward invariant amplitude for the $\gamma p \to \psi p \to e^- e^+ p$ process is given by

$$\mathcal{M}_\psi \simeq \frac{ie^3}{q'^2} \frac{f_\psi^2}{2M} \frac{1}{q'^2 - M_\psi^2 + iM_\psi\Gamma_\psi} T_{\psi p}$$
$$\times \left(\nu = \frac{1}{2}(s - M_\psi^2 - M^2) \right)$$
$$\times \varepsilon_\mu(q, \lambda) \cdot \bar{u}(l_-, s_-)\gamma_\nu v(l_+, s_+)$$
$$\times \bar{N}(p', s'_p)\left\{ \left(g^{\mu\nu} - \frac{q'^\mu q^\nu}{q \cdot q'} \right) + \frac{q \cdot q'}{(q \cdot P)^2} \right.$$
$$\left. \times \left(P^\mu - \frac{q \cdot P}{q \cdot q'}q'^\mu \right)\left(P^\nu - \frac{q \cdot P}{q \cdot q'}q'^\nu \right) \right\}N(p, s_p),$$

$$(22)$$

where $T_{\psi p}(\nu)$ is the forward ψp elastic scattering amplitude discussed above, and $\Gamma_\psi = 92.9 \pm 2.8$ keV is the total ψ width. Furthermore in Eq. (22), $u(v)$ denote the $e^-(e^+)$ spinors, N denotes the nucleon spinors, and ε_μ is the initial photon polarization vector. The expression of Eq. (22) corresponds to a near-forward approximation, as it involves the ψ-p amplitude $T_{\psi p}$ at $t = 0$, where terms of order $-t/s$ are neglected.

The $\gamma p \to \psi p \to e^- e^+ p$ cross section, differential in t, M_{ll}^2, and the electron solid angle $d\Omega^{e^- e^+ cm}$ in the c.m. frame of the dilepton pair is given by

$$\frac{d\sigma}{dt dM_{ll}^2 d\Omega^{e^- e^+ cm}} = \frac{1}{(2\pi)^4} \frac{1}{64(s - M^2)^2}$$
$$\cdot \frac{1}{4}\sum_\lambda \sum_{s_p} \sum_{s'_p} \sum_{s_-} \sum_{s_+} |\mathcal{M}_\psi|^2, \qquad (23)$$

with amplitude $\mathcal{M}_\psi$ given by Eq. (22). We performed the check that when integrating Eq. (23) over the electron solid angle and dilepton invariant mass, one obtains

$$\int dM_{ll}^2 \int d\Omega^{e^- e^+ cm} \frac{d\sigma}{dt dM_{ll}^2 d\Omega^{e^- e^+ cm}}\bigg|_{t=0}$$
$$= \left(\frac{\Gamma_{\psi \to ee}}{\Gamma_\psi} \right) \cdot \frac{d\sigma}{dt}\bigg|_{t=0} (\gamma p \to \psi p), \qquad (24)$$
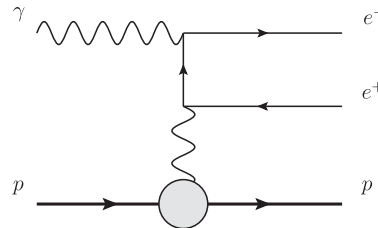

FIG. 5.   Dilepton ($e^+ e^-$) photoproduction through J/ψ (left) and Bethe-Heitler (right) processes.

with $d\sigma/dt|_{t=0}$ being the $\gamma p \to \psi p$ forward differential cross section given by Eq. (17), multiplied by the $\Gamma_{\psi \to ee}/\Gamma_{\psi}$ branching ratio.

An irreducible background to the above $\gamma p \to \psi p \to e^- e^+ p$ process arises from the BH process (Fig. 5, right). The BH invariant amplitude, contributing to the $\gamma p \to e^- e^+ p$ reaction, is given by

$$\mathcal{M}_{\mathrm{BH}} = \frac{ie^3}{t} \varepsilon^\mu(q,\lambda) \cdot \bar{N}(p',s_p')\Gamma^\nu N(p,s_p)$$
$$\times \bar{u}(l_-,s_-)\left\{\gamma_\mu \frac{\gamma \cdot (l_- - q) + m}{-2l_- \cdot q}\gamma_\nu \right.$$
$$\left. + \gamma_\nu \frac{\gamma \cdot (q - l_+) + m}{-2l_+ \cdot q}\gamma_\mu\right\} v(l_+,s_+), \quad (25)$$

with nucleon vertex given by

$$\Gamma^\nu = F_1(t)\gamma^\nu + F_2(t)\frac{i\sigma^{\nu\alpha}(p'-p)_\alpha}{2M}, \quad (26)$$

where $F_1(F_2)$ are the Dirac (Pauli) proton electromagnetic form factors, which we take from the recent fit of elastic e-p scattering data of Refs. [43,44]. In the presence of the Bethe-Heitler amplitude, the amplitudes $\mathcal{M}_\psi$ and $\mathcal{M}_{\mathrm{BH}}$ interfere, and the differential cross section is obtained by an analogous expression as Eq. (23), with the replacement $\mathcal{M}_\psi \to \mathcal{M}_\psi + \mathcal{M}_{\mathrm{BH}}$.

We next study this interference between ψ production and Bethe-Heitler mechanisms for typical kinematics of the $\gamma p \to e^- e^+ p$ process around the ψ production threshold, accessible at JLab [22–24]. In Fig. 6, we show the in-plane dilepton angles in the laboratory frame as a function of the
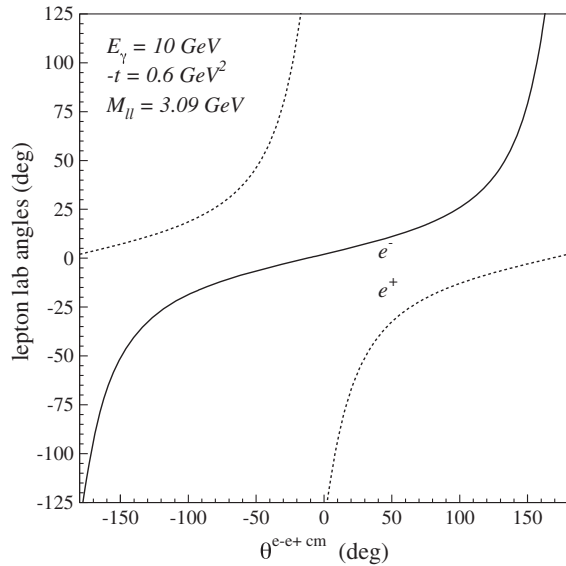
electron angle $\theta^{e^- e^+ cm}$, defined in the $e^- e^+$ c.m. frame, around the ψ resonance for JLab kinematics.

Figure 7 shows the differential cross section for the $\gamma p \to e^- e^+ p$ process around the ψ resonance. For selected values of the lepton angle ($\theta^{e^- e^+ \mathrm{cm}}$), we show the $\psi + \mathrm{BH}$ cross sections (denoted by forward angle cross sections), and compare them with the $\psi + \mathrm{BH}$ cross sections for the corresponding opposite lepton angle value ($\theta^{e^- e^+ \mathrm{cm}} - 180°$, denoted by backward angle cross sections). One notices a sizable interference in the lower tail of the ψ resonance.

We can directly access the real part of the ψ amplitude by exploiting this interference with the BH amplitude through the forward-backward asymmetry A_{FB} in the c.m. system of the dilepton pair. We consider the dilepton pair in the scattering plane defined by the two-body $\gamma p \to J/\psi p$ process, and define the asymmetry A_{FB} as

$$A_{\mathrm{FB}} \equiv \frac{d\sigma(\theta^{e^- e^+ \mathrm{cm}}) - d\sigma(\theta^{e^- e^+ \mathrm{cm}} - 180°)}{d\sigma(\theta^{e^- e^+ \mathrm{cm}}) + d\sigma(\theta^{e^- e^+ \mathrm{cm}} - 180°)}, \quad (27)$$

where $d\sigma$ stands for $d\sigma/dt dM_{ll}^2 d\Omega^{e^- e^+ \mathrm{cm}}$. This observable is 0 for both the BH process and the J/ψ process separately. Its nonzero value accesses the real part of the product of BH and J/ψ amplitudes.

Figure 8 shows the forward-backward asymmetry A_{FB} and its sensitivity on the subtraction constant $T_{\psi p}(0)$ in the

FIG. 6. Dilepton angles in the *lab* frame as a function of the electron angle $\theta^{e^- e^+ \mathrm{cm}}$, defined in the $e^- e^+$ c.m. frame. Solid (dashed) curves denote the $e^-(e^+)$ *lab* angles.
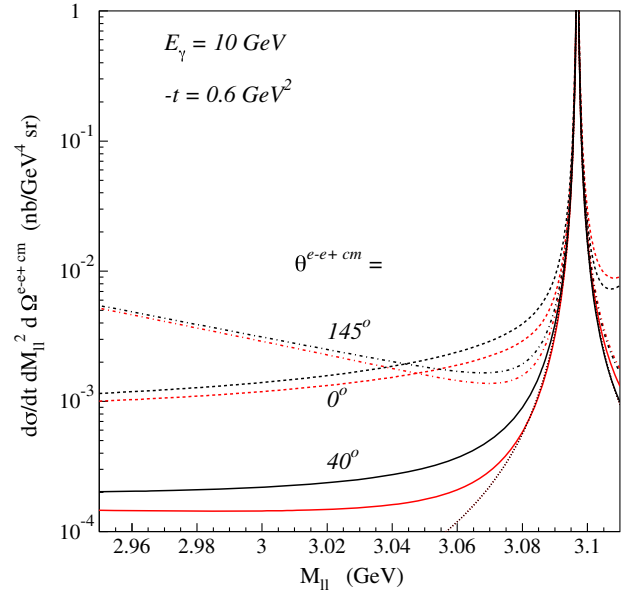

FIG. 7. Cross section for the in-plane $\gamma p \to e^- e^+ p$ process differential in t, M_{ll}^2, and electron solid angle $\Omega^{e^- e^+ \mathrm{cm}}$ in the dilepton c.m. frame, as a function of the dilepton mass M_{ll} around the ψ resonance, and for different values of the electron angle in the dilepton c.m. frame. The dotted curve denotes the ψ contribution. The other curves are the Bethe-Heitler + ψ results according to Eqs. (22) and (25) for $T_{\psi p}(0) = 22.45$. Lower red (upper black) curves show the forward (backward) angle cross sections.
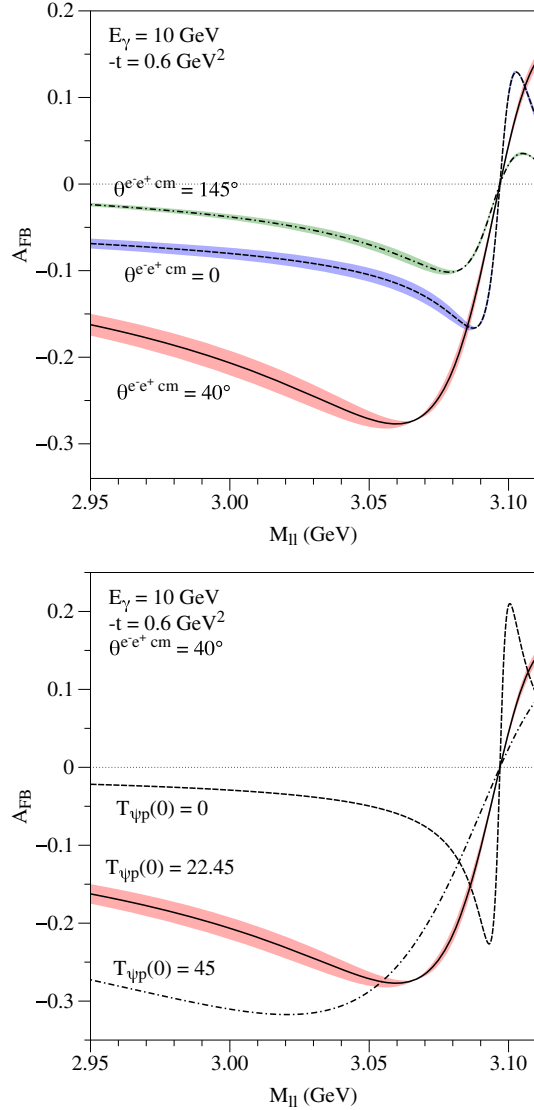
FIG. 8.   Forward-backward asymmetry for the $\gamma p \to e^- e^+ p$ process as a function of the dilepton mass M_{ll} around the ψ resonance. Dotted curve (corresponding with $A_{FB} = 0$): ψ contribution only. The other curves are the Bethe-Heitler + ψ results. Upper panel: Results for $T_{\psi p}(0) = 22.45$ and for different values of the electron angle in the dilepton c.m. frame. Lower panel: Results for $\theta^{e^- e^+ cm} = 40°$ and for different values of $T_{\psi p}(0)$. The bands represent the error resulting from our cross section fitting procedure.

kinematics of the JLab experiments. We notice that the asymmetry A_{FB} can reach values around -25% in these kinematics for the value $T_{\psi p}(0) = 22.45$ which was obtained in the fit above. In Fig. 8, we apply the same procedure of linear error propagation, mentioned above for the case of the cross section fits, to the asymmetry. Following this approach, the error of the asymmetry is estimated based on the first-order derivatives over the parameters,

$$\sigma^2_{A_{FB}} = \frac{\partial A_{FB}}{\partial \mathbf{p}} \cdot \Sigma_p \cdot \frac{\partial A_{FB}}{\partial \mathbf{p}}, \qquad (28)$$

where derivatives are taken at the fitted values of the parameters. We remark that in the particular case of the asymmetry all the derivatives become 0 at particular values of kinematical variables—the values at which the Bethe-Heitler cross section becomes equal to the ψ cross section. This is why our error bands show nodes at specific values of M_{ll}. One notices from Fig. 8 (lower panel) that away from the ψ resonance position, the asymmetry A_{FB} depends in good approximation linearly on the value of $T_{\psi p}(0)$. It therefore provides a very sensitive observable to extract $T_{\psi p}(0)$. A future measurement of A_{FB} at Jefferson Lab [22–24] may thus provide us with a clean way to extract $T_{\psi p}(0)$, or equivalently $a_{\psi p}$, and provide a cross-check of the value obtained from the cross section fits, as discussed in Sec. II.

IV. CONCLUSIONS

In this work, we provided an updated phenomenological analysis of the forward ψ-p scattering amplitude within a dispersive framework. Using VMD, we related the imaginary part of the forward ψ-p scattering amplitude to $\gamma p \to \psi p$ and $\gamma p \to c\bar{c}X$ cross section data. Furthermore, we calculated its real part through a once-subtracted dispersion relation. In our framework, the six parameters describing the discontinuities, and the one subtraction constant, are obtained from a global fit to both total and forward differential hidden and open-charm photoproduction cross sections. This fit allowed us to extract a value for the spin-averaged s-wave ψ-p scattering length $a_{\psi p} = 0.046 \pm 0.005$ fm, which can be translated into a ψ binding energy in nuclear matter of $B_\psi = 2.7 \pm 0.3$ MeV.

Starting from this $\gamma p \to \psi p$ amplitude we then calculated the $\gamma p \to \psi p \to e^- e^+ p$ process. This allowed us to estimate the forward-backward asymmetry for the $\gamma p \to e^- e^+ p$ process around the ψ resonance, which results from interchanging the leptons in the interference between the ψ production mechanism and the competing Bethe-Heitler mechanism.

This forward-backward asymmetry, which accesses the real part of the ψ-p amplitude, displays to good approximation a linear dependence on $a_{\psi p}$, away from the ψ resonance position. Using the forward $\gamma p \to \psi p$ amplitude obtained from our fitting procedure, we estimated that this forward-backward asymmetry can reach values around -25% for forthcoming ψ threshold electro- and photoproduction experiments at Jefferson Lab. Such forthcoming measurements can thus lead to a refined extraction of the ψ-p scattering length $a_{\psi p}$, and better constrain the ψ binding energy in nuclear matter.

ACKNOWLEDGMENTS

[1] D. Kharzeev, Proc. Int. Sch. Phys. Fermi **130**, 105 (1996).

[2] M. B. Voloshin, Prog. Part. Nucl. Phys. **61**, 455 (2008).

[3] A. Hosaka, T. Hyodo, K. Sudoh, Y. Yamaguchi, and S. Yasui, arXiv:1606.08685.

[4] S. J. Brodsky, I. A. Schmidt, and G. F. de Teramond, Phys. Rev. Lett. **64**, 1011 (1990).

[5] D. A. Wasson, Phys. Rev. Lett. **67**, 2237 (1991).

[6] M. E. Luke, A. V. Manohar, and M. J. Savage, Phys. Lett. B **288**, 355 (1992).

[7] M. E. Peskin, Nucl. Phys. **B156**, 365 (1979).

[8] S. J. Brodsky and G. A. Miller, Phys. Lett. B **412**, 125 (1997).

[9] S. H. Lee and C. M. Ko, Phys. Rev. C **67**, 038202 (2003).

[10] K. Tsushima, D. H. Lu, G. Krein, and A. W. Thomas, Phys. Rev. C **83**, 065208 (2011).

[11] A. Yokota, E. Hiyama, and M. Oka, Prog. Theor. Exp. Phys. **2013**, 113D01 (2013).

[12] A. Hayashigaki, Prog. Theor. Phys. **101**, 923 (1999).

[13] O. Lakhina and E. S. Swanson, Phys. Lett. B **582**, 172 (2004).

[14] A. B. Kaidalov and P. E. Volkovitsky, Phys. Rev. Lett. **69**, 3155 (1992).

[15] A. Sibirtsev and M. B. Voloshin, Phys. Rev. D **71**, 076005 (2005).

[16] K. Yokokawa, S. Sasaki, T. Hatsuda, and A. Hayashigaki, Phys. Rev. D **74**, 034504 (2006).

[17] T. Kawanai and S. Sasaki, Phys. Rev. D **82**, 091501 (2010).

[18] S. R. Beane, E. Chang, S. D. Cohen, W. Detmold, H.-W. Lin, K. Orginos, A. Parreo, and M. J. Savage, Phys. Rev. D **91**, 114503 (2015).

[19] D. Kharzeev and H. Satz, Phys. Lett. B **334**, 155 (1994).

[20] D. Kharzeev, H. Satz, A. Syamtomov, and G. Zinovjev, Eur. Phys. J. C **9**, 459 (1999).

[21] K. Redlich, H. Satz, and G. M. Zinovjev, Eur. Phys. J. C **17**, 461 (2000).

[22] Jefferson Lab Experiment, Report No. E12-12-006, https://www.jlab.org/exp_prog/proposals/12/PR12-12-006.pdf.

[23] Jefferson Lab Experiment, Report No. E12-12-001, https://www.jlab.org/exp_prog/proposals/12/PR12-12-001.pdf.

[24] Jefferson Lab Experiment, Report No. E12-16-007, https://www.jlab.org/exp_prog/proposals/12/PR12-16-007.pdf, https://phys.cst.temple.edu/~meziani/Pc_main-v2.pdf

[25] V. D. Barger and R. J. N. Phillips, Phys. Lett. **58B**, 433 (1975).

[26] K. Levenberg, Q. Appl. Math. **2**, 164 (1944).

[27] D. W. Marquardt, J. Soc. Ind. Appl. Math. **11**, 431 (1963).

[28] J. J. More, B. S. Garbow, and K. E. Hillstrom, Report No. ANL-80-74.

[29] B. Gittelman, K. M. Hanson, D. Larson, E. Loh, A. Silverman, and G. Theodosiou, Phys. Rev. Lett. **35**, 1616 (1975).

[30] U. Camerini, J. G. Learned, R. Prepost, C. M. Spencer, D. E. Wiser, W. W. Ash, R. L. Anderson, D. M. Ritson, D. J. Sherden, and C. K. Sinclair, Phys. Rev. Lett. **35**, 483 (1975).

[31] M. E. Binkley et al., Phys. Rev. Lett. **48**, 73 (1982).

[32] B. H. Denby et al., Phys. Rev. Lett. **52**, 795 (1984).

[33] P. L. Frabetti et al. (E687 Collaboration), Phys. Lett. B **316**, 197 (1993).

[34] S. Chekanov et al. (ZEUS Collaboration), Eur. Phys. J. C **24**, 345 (2002).

[35] K. Abe et al. (SLAC Hybrid Facility Photon Collaboration), Phys. Rev. D **30**, 1 (1984).

[36] A. R. Clark et al., Phys. Rev. Lett. **45**, 682 (1980).

[37] J. J. Aubert et al. (European Muon Collaboration), Nucl. Phys. **B213**, 31 (1983).

[38] M. I. Adamovich et al. (Photon Emulsion Collaboration), Phys. Lett. B **187**, 437 (1987).

[39] M. Derrick et al. (ZEUS Collaboration), Phys. Lett. B **349**, 225 (1995).

[40] J. J. Aubert et al. (European Muon Collaboration), Phys. Lett. **89B**, 267 (1980).

[41] R. Aaij et al. (LHCb Collaboration), Phys. Rev. Lett. **115**, 072001 (2015).

[42] Q. Wang, X. H. Liu, and Q. Zhao, Phys. Rev. D **92**, 034022 (2015).

[43] J. C. Bernauer et al. (A1 Collaboration), Phys. Rev. Lett. **105**, 242001 (2010).

[44] J. C. Bernauer et al. (A1 Collaboration), Phys. Rev. C **90**, 015206 (2014).